Transversely Compressed- and Restrained Shear Joints

Schmidt, Jacob Wittrup; Hansen, Christian Skodborg

Published in:
Proceedings of the 11th International symposium on fiber reinforced polymers for reinforced concrete structures

Publication date:
2013

Transversely Compressed- and Restrained Shear Joints

J. Wittrup Schmidt[1], C. Skodborg Hansen[2]
[1]Danish technical university, Brovej, Bygning 118, 2800 Kgs. Lyngby, jws@byg.dtu.dk
[2]Danish technical university, Brovej, Bygning 118, 2800 Kgs. Lyngby, csh@byg.dtu.dk

Keywords: Analytical analysis, Reinforced concrete, Debonding, Structural design, Laminate, CFRP, Flexural strengthening, Joint, Bond tests.

SUMMARY
Anchorage of FRP strengthening systems where the deformation perpendicular to the FRP material is restrained or a compressive force is applied on the strengthening, seems to provide ductility, increased utilization of the FRP and failure modes which can be controlled through the anchorage method. This paper presents theoretical model which can predict the response of transversely compressed and restrained single- and double lap shear joints. The interface material model is based on a cohesive law in the shear-slip plane with a descending branch and a uniform frictional stress added due to the friction in the crack, emanating from the transverse pressure or restraint. The theoretical model is compared with experimental results from transversely compressed single- and double shear joints. Also theoretical predictions of a mechanical integrated sleeve-wedge anchorage load capacity are carried out and compared with tests. It is seen that the theory correlates well with the experimental results.

1. INTRODUCTION
FRP (Fibre Reinforced Polymers) strengthening of concrete structures has been used efficiently during the last decades. FRP materials usually offer high strength, low weight and desirable corrosion properties which enables them to be applied externally on a civil structure. In addition, these strengthening systems can be manufactured with different cross section geometries, where the most common are FRP- plates, sheets and bars. The combination of fibre and resin in the FRP provides a material which is linear elastic until failure, also resulting in stiffness and strength which can be tailored through the fibre/resin ratio.
When a FRP material is applied to a concrete structure, the load capacity is dependent on sufficient bond between the FRP materials and concrete. Since this bond often is sufficient, tensile crack propagation in the concrete occurs, causing premature failure where IC (intermediate crack) de-bonding or concrete separation can be the outcome [1-4]. As a consequence the FRP is not fully utilized. Additionally, sufficient ductility of the strengthened member seems to be a shortcoming, which makes the consulting engineer reluctant to use FRP strengthening systems. Significant research concerning anchorage of Carbon FRP plates and bars has therefore been ongoing in the recent years. It is from these studies seen that mechanical anchorages offer a good solution to the de-bonding issue. S.T. Smith [5] used CFRP anchorages made of rolled fibre sheet dowels to anchor FRP plates to a RC slab. The anchorages were placed in different configurations and fibre content in the FRP anchorages was changed too. It was in all tests seen that ductility was increased and some of the tests also showed a significant increase in load capacity compared to the unanchored strengthening configuration. The greatest enhancement in load and deflection experienced by the slabs strengthened with FRP plates and anchored with FRP anchors was 30% and 110%, respectively, compared to the unanchored FRP-strengthened control slab. Other solutions such as embedded metal threads [6], hybrid bonding (nailed

plates) [7]), U-jackets [8], Anchorage of multidirectional Carbon FRP plates using metallic bolts [16], are related examples.
Mechanical anchorage of CFRP tendons in a post-tensioning setup is also a way to provide strengthening. Such external cable strengthening also to provide a higher magnitude of ductility and strength provided sufficient anchorage of the Carbon FRP [9], [10]. Equal for these mechanical anchorage used for plates- and tendons is the interface between the adherents which is compressed and/or enclosed by a FRP fan or wedge, a transverse pressure- or restraining mechanism which is desirable when increased ductility and better utilization of the FRP is the objective.

1.1 Transversely compressed and restrained joints

A shortcoming is however research concerning the effect of transverse compression or restraining applied to bonded joints. Transverse pressure enables friction in the cracked interface and changes the principal stress direction. Pichler [11] studied the effect of transversely compressed steel to concrete joints, in connection with anchorage of steel plates to concrete beams. The study showed increase of the anchorage capacity when transverse pressure was applied. Analysis of the joint was performed using NLFM (Non Linear Fracture Mechanics), with a bond-slip model shaped as an ascending power law. The maximum shear strength used in the power law was multiplied a contribution from the compression, derived from the principal stress state in the compressed bond line. The model did not include friction or consideration of the mixed mode state in the interface.
In Simonsen and Brincker [12] friction was introduced directly into a cohesive law describing an interface between a steel fiber and concrete. A model for fiber pull-out was proposed using this law, and NLFM was used for the theoretical analysis. The model did not include the concrete stiffness. When a crack is propagating in a granular material or interface in mode II, the non-smooth fracture surface will introduce deformations perpendicular to the pull-of direction, and create a mixed mode state in the interface and at the crack tip. To the author's knowledge, only limited attention has been on evaluation of this mixed-mode failure and dilatation effect in bonded joints. However, some numerical implementations in finite element programs exists, see [13,14]. The combined tension-shear fracture is in itself difficult to describe, but when compression is added to the interface with a loading device that also hinders outward movement, see Pichler [11], an additional dilatation induced compression appears on the interface. The magnitude of the dilatation induced compression is not investigated in this paper, but it will depend on the roughness of the interface and stiffness of the device introducing the pressure.

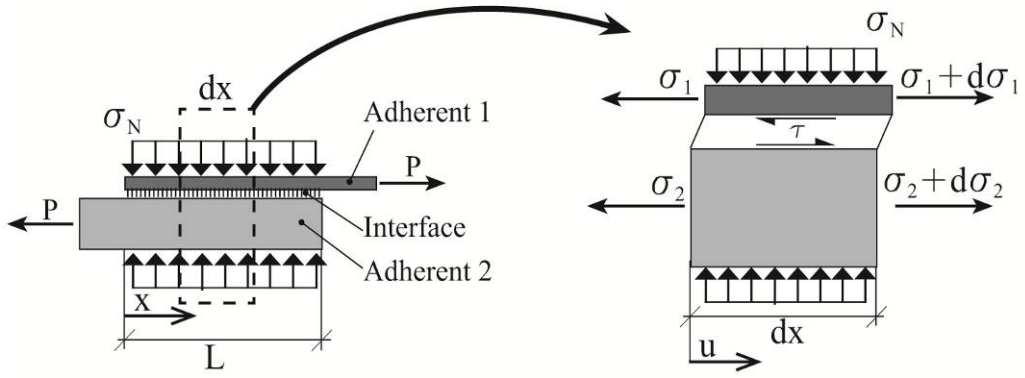

Figure 1: Infinitesimal element of a bonded joint with transverse compressive stress on the interface.

This paper presents a theoretical model, which predicts the response of bonded joints where transverse pressure applied to interface on the surface of the adherents, Figure 1. The transverse pressure is accounted for by a cohesive law incorporating a Coulomb friction contribution. The cohesive law, Figure 2, is used to describe the interface, is a special case of the bond-slip law used in Simonsen and Brincker [12]. It is defined as a linear descending branch followed by a horizontal plateau created by Coulomb friction in the interface, depending on the magnitude of the transverse pressure. In Simonsen and Brincker the stiffness of only one adherent is considered, whereas the model in this paper

incorporates both adherents. More information concerning theory and tests, used in this paper, can be found in [15].

2. THEORY

The interface material model used for the joint analysis, is a cohesive law in the shear-slip plane, with a descending branch originating from s(0) = τ_m. A uniform frictional stress $\Delta\tau$ is added due to the friction in the crack, emanating from the transverse pressure σ_N on the joint, Figure 1. When the crack propagates in concrete, another possible interpretation of $\Delta\tau$ is based on Coulomb's friction hypothesis. It is seen how the friction can increase the maximum shear stress from τ_m to τ_p depending on the angle of friction θ. This relation can be written:

$$\tau_p = \tau_m + \sigma_N tan(\theta) = \tau_m + \mu\sigma_N = \tau_m + \Delta\tau \tag{1}$$

$$\tau(s) = \begin{cases} \Delta\tau + \tau_m\left(1 - \frac{s}{s_0}\right) & for\ 0 < s \leq s_0 \\ \Delta\tau & for\ s_0 < s \leq s_\infty \end{cases} \tag{2}$$

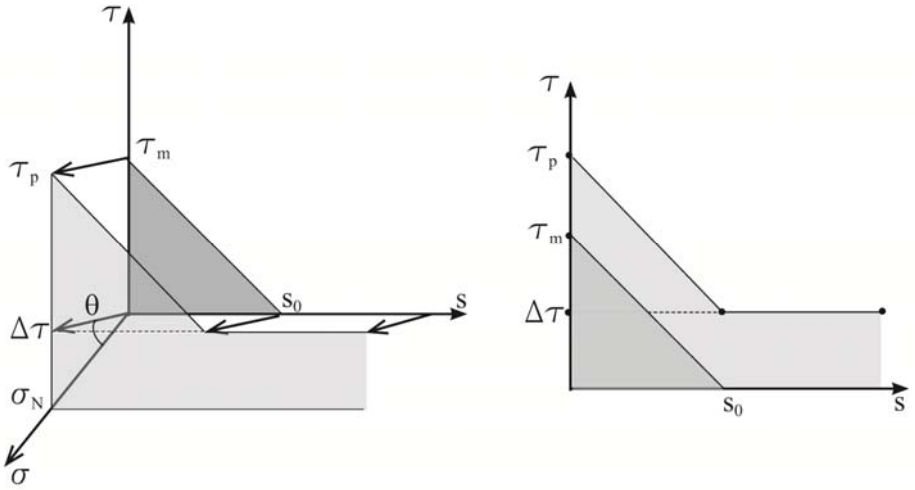

Figure 2: Descending cohesive material model with a contribution from friction

During the general derivation, geometry and other definitions are found in Figure 1. The adherents are linear elastic and by assuming only small strains we can write:

$$\epsilon_1 = \frac{\sigma_1}{E_1} \tag{3}$$

$$\epsilon_2 = \frac{\sigma_2}{E_2} \tag{4}$$

Considering this infinitesimal element, the following horizontal equilibrium conditions may be written for both adherents as:

$$\frac{d\sigma_1}{dx} - \frac{\tau}{\tau_1} = 0 \tag{5}$$

$$\frac{d\sigma_2}{dx} - \frac{\tau}{\tau_2} = 0 \tag{6}$$

The kinematic conditions derived, results in:

$$\varepsilon_1 = -\frac{du_1}{dx} \tag{7}$$

$$\varepsilon_2 = -\frac{du_2}{dx} \tag{8}$$

Defining the positive slip in the interface as the difference in deformation between adherents as

$$s = u_1 - u_2 \tag{9}$$

Differentiating (9) once with respect to x gives us

$$\frac{ds}{dx} = -\frac{du_1}{dx} - \frac{du_2}{dx} \tag{10}$$

Using Eqs. (3) and (4) in (10) results in

$$\frac{ds}{dx} = \frac{\sigma_1}{E_1} - \frac{\sigma_2}{E_2} \tag{11}$$

Differentiating once more and applying (5) and (6) provides

$$\frac{d^2s}{dx^2} - \omega_1^2\,\tau(s) = 0 \tag{12}$$

where

$$\omega_1^2 = \left[\frac{1}{E_1 t_1} + \frac{1}{E_2 t_2}\right] \tag{13}$$

It will later prove beneficial to introduce the constant

$$\omega_2^2 = \frac{\tau_m}{s_0}\omega_1^2 \tag{14}$$

It is now possible to write the differential equations valid for the softening and friction part of the cohesive law when substituting Eq. (2) into Eq. (12). Theoretical expressions for the shear stress, slip and force are derived in different stages of crack propagation (a–d), Figure 3. The elastic region of the joint is denoted [E]. Softening regions of the joint is denoted [S]. Regions where only friction is present is denoted [F], and [D] is the Debonding region.

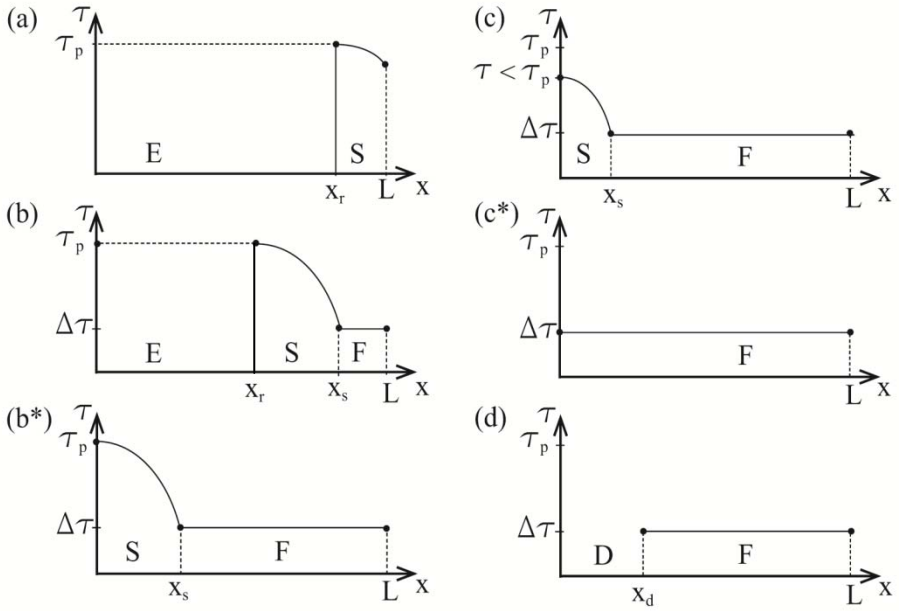

Figure 1: Fracture regimes: (a) elastic–softening, (b) elastic–softening–friction, (b*) full softening-friction, (c) softening-friction, (c*) full friction, (d) debonding-friction.

2.1 Elastic-Softening (a)

The elastic–softening stage describes the beginning of crack propagation. A point $x = x_r$ to the end of the elastic region of the joint is defined, describing the size of the elastic zone. At this distance the assumption of no elastic contribution provides the boundary condition $s(x_r) = 0$. Since we have no elastic deformation, a second boundary is obtained knowing equal strain state exists in the adherents at $x = x_r$. It is then implicitly given that $ds(x_r)/dx = 0$. Using these boundary conditions, results in following expressions describing the slip, shear and force:

$$s(x) = \frac{s_0 \tau_p (1 - \cos(\omega_2 (x - x_r)))}{\tau_m} \tag{14}$$

Inserting in Eq. (2) gives the shear stress

$$\tau(x) = \tau_p cos(\omega_2 (x - x_r)) \tag{15}$$

The force can be found by using $ds/dx = P/E_1 t_1$ at $x = L$.

$$P = \left[1 + \frac{E_1 t_1}{E_2 t_2}\right] \frac{\tau_p \sin(\omega_2 (L - x_r))}{\omega_2} \tag{16}$$

2.2 Elastic-Softening-friction (b)

When x_r has been moved towards $x = 0$, the slip exceeds $s(L) = s_0$ and shear stress attains a pure friction state at $x = L$. Eqs. (14) and (15) may be reused in the interval $x_r \leq x < x_s$, because similar boundary conditions have to be used. x_s is found by solving $s(x_s) = s_0$ for x_s. Using Eq. (14) for this purpose provides the expressions describing slip and shear.

$$s(x) = s_0 + \frac{\Delta\tau\, \omega_1^2 (x - x_s)^2}{2} + \frac{\tau_p}{\tau_m} s_0 \omega_2 \sin(\omega_2 (x_s - x_r))\,(x - x_s)) \tag{17}$$

$$\tau(x) = \Delta\tau \tag{18}$$

The force can be found by using $ds/dx = P/E_1 t_1$ at $x = L$.

$$P = \left[1 + \frac{E_1 t_1}{E_2 t_2}\right] \left[\frac{\tau_p \sin(\omega_2 (x_s - x_r))}{\omega_2} + \Delta\tau (L - x_s)\right] \tag{19}$$

It is now possible to write the expression for force partly as a function of the fracture energy. Inserting x_s into Eq. (19) and rearranging, we obtain the expression:

$$P = \left[1 + \frac{E_1 t_1}{E_2 t_2}\right] \left[\sqrt{\frac{2G_f}{\omega_1^2}} + \Delta\tau (L - x_s)\right] \tag{20}$$

The fracture energy G_f is defined as the area engulfed by the cohesive law from $s=0$ to $s=s_0$.

$$G_f = \frac{s_0}{2}(2\Delta\tau + \tau_m) \tag{21}$$

2.3 Full Softening-friction (b*)

When the crack has propagated through the entire joint and $x_r = 0$, the maximum capacity of the joint is found. The expression for force is similar to Eq. (19), but the expression for x_s, may be simplified to:

$$x_s = \frac{\left[\pi - cos^{-1}\left(\frac{\tau_m - \tau_p}{\tau_p}\right)\right]}{\omega_2} \tag{22}$$

2.4 Softening-friction (c)

After reaching stage (b*), the remaining degraded region from x=0 to x=x_s will continue degrading. The response for stage (c) is found by imposing a slip value, s(0) = s_e, ranging from 0 to s_0 in magnitude.

The elastic zone is vanished since $x_r = 0$, and we have a fictitious crack spanning the entire length of the bond line. This will result in shear stresses $\tau < \tau_p$ at x = 0. Initial conditions are chosen as: s(0) = s_e and $ds_S(0)/dx = 0$. The slip can then be expressed as:

$$s(x) = \frac{-cos\,(\omega_2 x)(s_0\tau_p - s_e\tau_m)}{\tau_m} + \frac{\tau_m}{\tau_p}s_0 \tag{23}$$

Shear stress is found by insertion in Eq. (2). For the friction region we have the initial conditions $s(x_s) = s_0$ and $ds_S(x_s)/dx = ds_F(x_s)/dx$. These boundary conditions provide:

$$s(x) = \frac{\Delta\tau\,\omega_1^2(x - x_s)^2}{2} + \frac{\omega_2 sin(\omega_2 x_s)(x - x_s)(s_0\tau_p - s_e\tau_m)}{\tau_m} + s_0 \tag{23}$$

The force is found by using the first derivative of the slip in the friction region of the interface at x = L, and isolating P in $ds_F(L)/dx = P/E_1t_1$. After re-arranging we obtain the expression for P:

$$P = E_1t_1\left[\Delta\tau\omega_1^2(L - x_s) + \frac{\omega_2\,\sin(\omega_2 x_s)\,(s_0\tau_p - s_e\tau_m)}{\tau_m}\right] \tag{24}$$

To find the position of x_s, we isolate x_s when inserting $s(x_s) = s_0$ in the softening region.

$$x_s = \frac{\left[\pi - cos^{-1}\left(\frac{s_0(\tau_m - \tau_p)}{s_0\tau_p - s_e\tau_m}\right)\right]}{\omega_2} \tag{22}$$

2.5 Full friction (c*)

Stage (c*) where $s_e = s_0$ is a special case of stage (c). Inserting $s_e = s_0$ gives us the following result:

$$P = \left[1 + \frac{E_1t_1}{E_2t_2}\right]\Delta\tau L \tag{23}$$

2.6 Full friction (d)

In stage (d), the adherent 1 is pulled of adherent 2, while only friction from the transverse pressure on the crack contributes to the load capacity. At the left end from x = 0 to x = x_d, a free surface is created due to debonding. The response is found by changing the length of the completely debonded region, x_d. Initial conditions are chosen as $s(x_d)=s_0+x_d$ and $ds(x_d)/dx=0$. With the given boundary conditions we obtain

$$s(x) = \frac{\Delta\tau\,\omega_1^2 x(x - 2x_d)}{2} + x_d + s_0 \tag{24}$$

Shear stress and force is calculated using $ds/dx = P/E_1t_1$ at x = L.

$$\tau(x) = \Delta\tau \tag{25}$$

$$P = \left[1 + \frac{E_1 t_1}{E_2 t_2}\right] \Delta\tau (L - x_d) \tag{26}$$

3. RESULTS

Results are presented using the following material parameters: E_1 = 156 GPa; E_2 = 38.6 GPa; t_1 = 1.6 mm; t_2 = 400 mm; s_0 = 0.35 mm; $\Delta\tau$ = 2 MPa; s_m = 5 MPa; L = 400 mm. The joint will reach 4 different stages of crack propagation, stages (a–d) as seen from Figure 4a. In stage (a), we see the first onset of crack propagation. It ends when the slip value exceeds $s(L) = s_0$ and a region of the bonded surface will be solely in friction. The friction provides the inclination of the otherwise horizontal curve in stage (b). At the end of stage (b) the maximum load is reached. Stage (c) follows with the final degradation of the remaining descending part cohesive law, leaving only the friction contribution behind at the end. The presented example shows elastic unloading or snap-back behaviour. This is due to the chosen bond length. Smaller bond lengths may avoid snap-back behaviour. Stage (d) shows the friction contribution which is present until the interface is fully debonded. The debonding process continues until full separation. Figure 4b and 6a shows the effect of the added friction, where 6 different values of $\Delta\tau$ are presented ranging from 0 to 5 MPa. With $\Delta\tau$ = 0 MPa we find the classic behaviour of a cohesive descending law without any frictional contribution. When applying friction in the magnitude of the shear strength τ_m of the interface, it can be seen that the maximum load is increased significantly, along with a substantial increase in slip. When performing the parametric study by changing $\Delta\tau$ on the bonded length of a lap-joint, it is found that the joint will reach a limit for transferable load, the so-called anchorage length, even if the length of the joint is increased. When this load is reached, steady state crack propagation occurs. Also, when a cohesive law contains a friction contribution, the load will continue to increase as long as there is an uncracked interface in which the crack may propagate. In the case without friction, no further increase in maximum load at large bond lengths will occur. However when friction contribution and pressure is applied, the maximum load increases. The combination of friction contribution and extended anchorage length is predicted to increase the load capacity significantly compared to the case without friction.

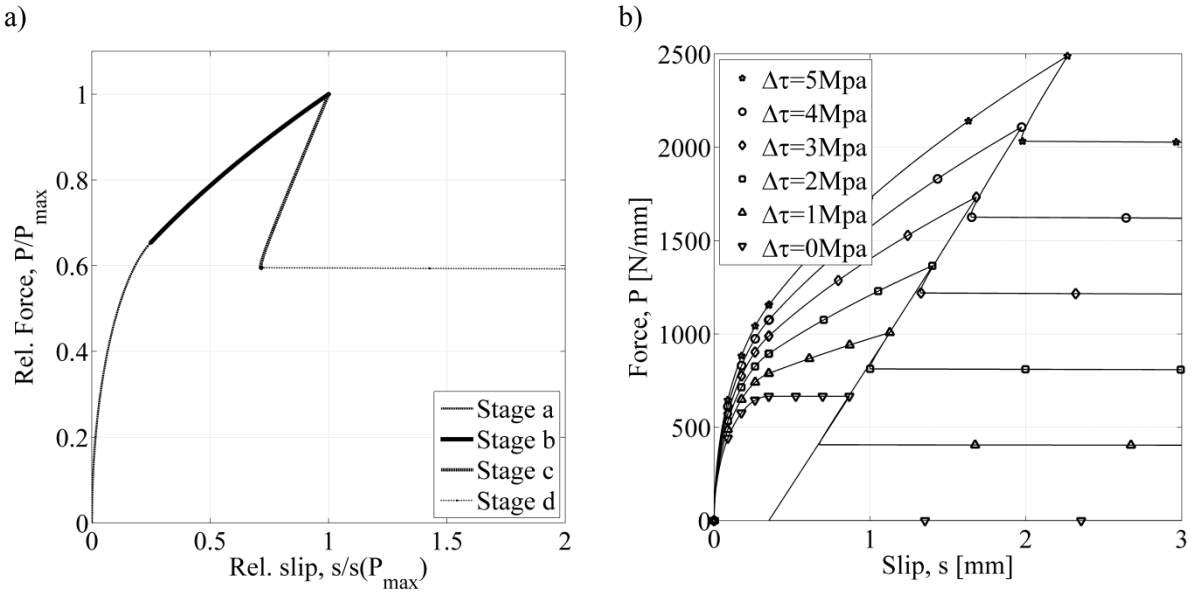

Figure 4: a) Load normalized with max. load (P_{max}) as a function of slip (at x = L) normalized with slip value at max load ($s(P_{max})$). b) Load versus slip at different friction contributions, $\Delta\tau$.

3.1 Tests and theory: Transversely compressed single- and double shear joints

The theory is compared to 59 shear tests performed by Pichler [11]. 53 of the tests comprised single shear push–pull joints and 6 tests were performed on a double shear pull-pull joint setup, Figure 5a and 5b respectively. Pressure on the steel was applied using a compressing plate anchored with concrete anchorages and controlled through either wrench moment or strain gauge measurements on

the anchor rods. Lubricant was used in the interface between the compressing plate and steel clamp to reduce friction. Tensioning of the steel was performed until joint failure. It was noticed that the pressure had an effect on the location of fracture line (concrete, adhesive or adhesive/steel interface).

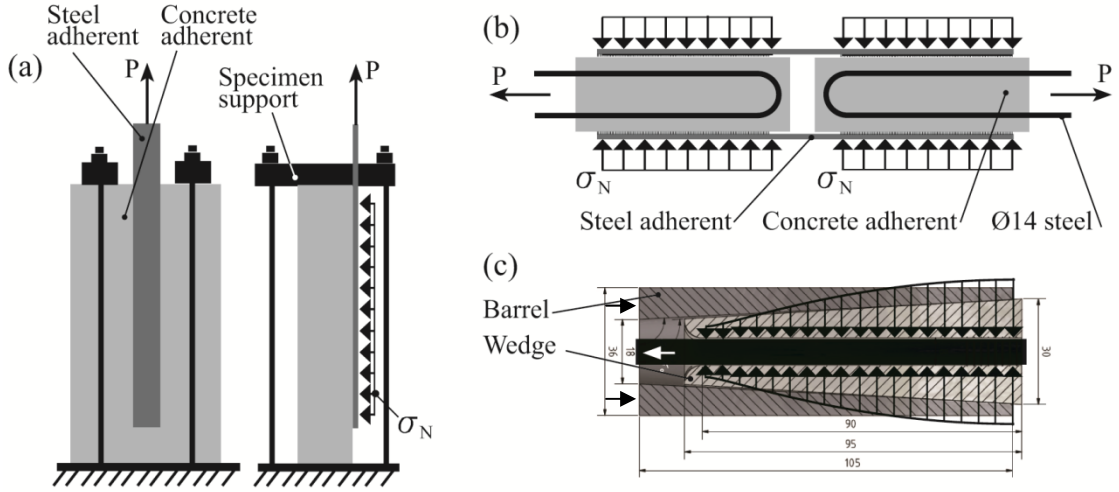

Figure 5: a) Single shear joint configuration. b) Double shear joint configuration. c) Example of pressure in restraint and compressed integrated sleeve-wedge anchorage.

It is seen from Figure 6b, that the theoretical maximum capacity predicts the same tendency as in the tested specimens, but underestimates the results with approximately 16%. There are one group of tests that differ significantly. Specimens 31.1–33.1, which consisted of concrete with a lower compression strength, are in average 30% below the predicted load. The squared correlation coefficient, R^2, is used to validate the test results. The calculated value of $R^2 = 0.922$ indicate a strong correlation between tests and theory. This together with the data from figure 6b suggests a correct behaviour of the proposed model.

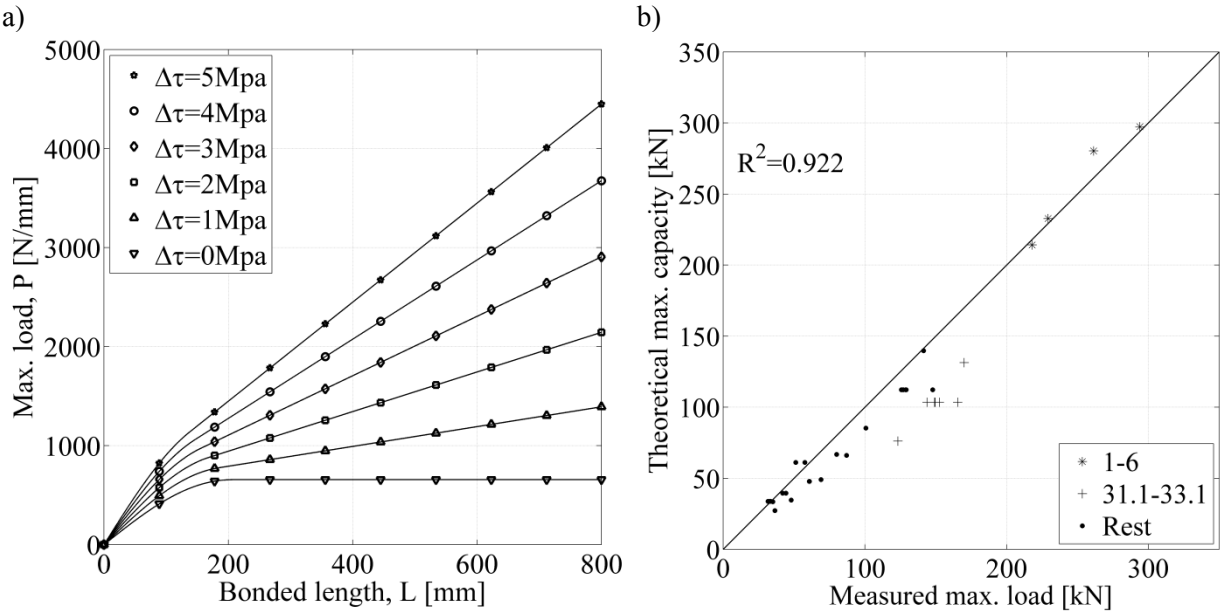

Figure 6: a) Analytically predicted bond length, b) Analytical maximum loads compared to experimental results

3.1 Tests and theory: Enclosed transversely restrained CFRP rod

Theory and tests also seems to correlate well when used to evaluate a novel mechanical integrated sleeve wedge anchorage, Figure 5c and 7b [10]. Implementing, E_1=140GPa, E_2=150GPa, s_o=0.05,

t_1=11mm, t_2=4mm, τ_m=25MPa and a pressure related to the investigated anchorage component (derived in the commercial program ABAQUS), enables calculation of the ultimate anchorage capacity. Here anchorage bond lengths of 70mm, 90mm with different pressure curves applied to the CFRP/wedge interface was investigated. Stage b*), where the highest joint capacity is reached, was compared to experimental results. The theory is developed for the use of a uniform transverse pressure. It is however seen that the anchorage applies a non-uniform pressure in order to reduce the principal stress magnitude (from tension and transverse compression) along the anchorage. The transverse pressure therefore has to be transformed into a uniform pressure, Figure 7a. This approach was assumed to be satisfactory when using the theory to predict the tests results.

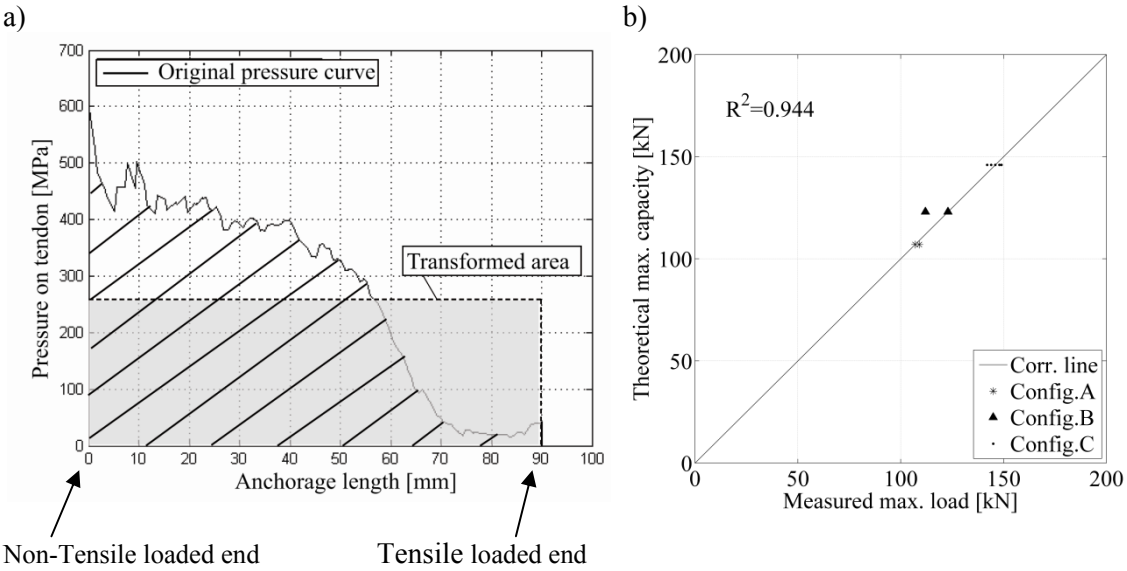

Figure 7: a) Example of pressure transformation into an even distribution (the loaded end is where the full tendon/rod load is applied to the mechanical anchorage) and b) Correlation between tests performed on the integrated sleeve-wedge anchorage and theory

Fracture was seen to occur in the CFRP adhesive surface layer. A shortcoming was however the manufacturer's value for the matrix shear capacity, τ_m. As a consequence this value is assumed and the model is calibrated to fit the configuration C experimental results. After this is done, the capacity of configuration A and B is predicted by changing the anchorage length and pressure only. It is seen from the correlation coefficient that the theory correlates well with the test results. However, the coefficient is based on relatively few tests in each configuration. More tests should therefore be carried out, using variable pressures- and anchorage lengths to get a better indication of the applicability of the developed theoretical model, as an evaluation method for the friction anchorage.

4 CONCLUSIONS

A bonded joint loaded in tension with transverse pressure applied on the bonded interface, was analyzed using a cohesive law incorporating a Coulomb friction contribution for the interface. It was shown that transverse pressure on a bonded interface results in increased load capacity. The theory also predicts an increased ductile behaviour of bonded joints when the transverse pressure is of significant magnitude, which is a desirable behaviour in structures. The analytical model was compared to experiments performed by Pichler [11]. The load capacity of the test specimens tested with a concrete compression C25/30 and C50/60 was predicted 16% lower than the tested maximum load in average. It was however seen that specimens 31.1–33.1, which consisted of concrete with a compression strength of C16/20, were 30% below the predicted load. Within this average are some experiments that deviated significantly from other groups of tests. With this in mind and the fact that not all experimental details are known, it can be concluded that the analytical model predicted the

maximum load with a good accuracy. No curve fitting factors to improve the mean error has been used, which is often seen in similar research. Furthermore the coefficient of determination calculated as 0.922 is close to one, indicating a strong correlation between tests and theory. The load capacity and semi-ductility seems highly dependent on the friction contribution, $\Delta\tau$. When comparing joints with equal bond lengths with- and without transverse pressure, the compressed joint will reach a higher load capacity. It is also possible to shorten the necessary bond length, since a compressed joint is able to transfer the same force over a shorter distance. Also when predicting the maximum load of the enclosed transversely compressed CFRP rod a good correlation between theory and experiments, was found. More tests are however needed. The model is therefore deemed to be a useful tool for evaluation of different joint configurations, using compression- and/or restraints in the anchorage configuration. The theory, in general, shows to correlate well with tests, and may serve as a good engineering tool for evaluation of transversely compressed and restrained bonded joints.

REFERENCES

[1] Täljsten, B.” Strengthening of Beams by Plate Bonding.” J. Mater. Civil Eng., Vol 9, No 4, pp. 206-212, (1997).
[2] T.C. Triantafillou, C.P. Antonopolos. “Design of concrete flexural members strengthened in shear with FRP” J. Compos. Constr., Vol 4, No 4, 198-205, (2000).
[3] J.G. Teng “Intermediate crack-induced debonding in RC beams and slabs” J. of Constr. and Build. Mat., Vol 17, No 6, 447-462, (2003)
[4] H. Said and Z. Wu “Evaluating and Proposing Models of Predicting IC Debonding Failure.” J. Compos. Constr., Vol. 12, No. 3, 284-299, (2008).
[5] S.T. Smith, S. Hu, S.J. Kim, R. Seracino, “FRP-strengthened RC slabs anchored with FRP anchors” J. of Engineering Structures 33, 1075–1087, (2011)
[6] A. Sharif, G.J. Al-Sulaimani, I.A. Basunbul, M.H. Baluch, B.N. Ghaleb ”Strengthening of initially loaded reinforced concrete beams using FRP plates” ACI Struct J., Vol. 91, No 2, 160–8, (1994).
[7] Y.C. Yun, Y.F. Wu, W.C. Tang ”Performance of FRP bonding systems under fatigue loading” Eng Struct, Vol. 30, No 11, 3129–40, (2008).
[8] S.T. Smith, J.G. Teng ”Shear-bending interaction in debonding failures of FRPplated RC beams”. Adv. Struct. Eng., Vol 6, No. 3, 183–99, (2003).
[9] C.K. Ng, and K.H. Tan “Flexural behaviour of externally prestressed beams. Part I: Analytical model,” Eng. Struc., Vol. 28, No. 4, 609-621, (2006).
[10] J.W. Schmidt “External strengthening of building structures with prestressed CFRP” Ph.D. thesis, Denmark, Danish technical university, Dept. of civil Engineering, Report R-230 2011, ISBN 9788778773098.
[11] D. Pichler” Die Wirkung von Anpressdrncken auf die Verankerung von Klebelamellen” (in German). Ph.D. thesis, Universit., St Innsbruck; (1993).
[12] J. Simonsen, R. Brincker ”Influence on the shear-slip relation on the fibre bridging curve in FRC”. In: Brandt A, Li VC, Marshall IH, editors. Brittle matrix composites 5, (1997).
[13] I. Carol, P.C. Prat ”Normal/shear cracking model: Application to discrete crack analysis” J. Eng Mech, Vol. 123, No. 8, 765-773, (1997)
[14] L.O. Nielsen, J.F. Mougaard, J.S. Jacobsen, P.N. Poulsen ”A mixed mode model for fracture in concrete”. FRAMCOS-7 symposium, Korea, 231–7, (2010)
[15] C.S. Hansen, J.W. Schmidt, H. Stang” Transversely compressed bonded joints”. Comp.: Part B., Vol. 43, 691–701, (2012).
[16] L. Brunckhorst, PJ Knudsen, E. Poulson E, T. Thorsen ”Forstærkning af betonkonstruktioner med bolte-limede kulfiberbånd” En elementær teknisk introduktion. Esbjerg (Denmark): Rosendahls ogtrykkeri A/S, in Danish, (2007).